Aerosp. Sci. Technol. 5 (2001) 95–108
© 2001 Éditions scientifiques et médicales Elsevier SAS. All rights reserved
S1270-9638(00)01090-7/FLA

The turbulent decay of trailing vortex pairs in stably stratified environments

Frank Holzäpfel *, Thomas Gerz, Robert Baumann

Institut für Physik der Atmosphäre, DLR Oberpfaffenhofen, 82234 Weßling, Germany

Received 4 April 2000; revised and accepted 22 November 2000

Abstract

The decay of trailing vortex pairs in thermally stably stratified environments is investigated by means of large eddy simulations. Results of in-situ measurements in the wakes of different aircraft are used to find appropriate intitializations for the simulation of wake turbulence in the quiescent atmosphere. Furthermore, cases with weak atmospheric turbulence are investigated. It is shown that the early development of the vortices is not affected by turbulence and develops almost identically as in 2D simulations of wake vortices in stably stratified environments. In a quiescent atmosphere the subsequent vortex decay is controlled by the interaction of short-wave disturbances, owing to the aircraft induced turbulence, and baroclinic vorticity, owing to stable stratification. As a consequence, vertical vorticity streaks between the vortices are induced which are substantially intensified by vortex stretching and finally lead to rapid turbulent wake-vortex decay. When in addition atmospheric turbulence is also present, the long-wave instability is dominantly promoted. For very strong stratification ($Fr < 1$) it is observed that wake vortices may rebound but lose most of their strength before reaching the flight level. Finally, the simulation results are compared to the predictive capabilities of Greene's approximate model. © 2001 Éditions scientifiques et médicales Elsevier SAS

wake vortices / stable stratification / turbulence / short-wave instability / coherent structures / numerical simulation

Zusammenfassung

Turbulent zerfallende Nachlaufwirbel in stabil geschichteter Umgebung. Der turbulente Zerfall von Flugzeug-Wirbelschleppen in thermisch stabil geschichteter Umgebung wird mittels der Grobstruktursimulation untersucht. Die Parametrisierung der Turbulenz in den Nachlaufwirbeln wird von in situ Messungen abgeleitet, die im Nachlauf verschiedener Flugzeuge durchgeführt wurden. Weiterhin werden Fälle mit schwacher atmosphärischer Turbulenz untersucht. Zunächst bleiben die Wirbel von der Turbulenz unbeeinflußt; sie verhalten sich nahezu wie in 2D Simulationen von Wirbelschleppen in stabil geschichteter Umgebung. Der anschließende Zerfallsprozess wird in nicht turbulenter Umgebung durch die Wechselwirkung kurzwelliger Störungen und baroklin erzeugter Wirbelstärke geprägt. Zwischen den Nachlaufwirbeln werden vertikale Wirbelröhren induziert, die zunächst durch Wirbelfadenstreckung maßgeblich verstärkt werden und schließlich einen rapiden turbulenten Zerfall der Wirbelschleppe initiieren. In einer Umgebung mit atmosphärischer Turbulenz dominiert die langwellige Instabilität. In sehr stabiler Schichtung ($Fr < 1$) können die Wirbel zwar bis auf Flugniveau wiederaufsteigen, jedoch verklingt ihre Intensität gleichzeitig nahezu vollständig. Abschließend wird das Vorhersagepotential von Greene's parametrischem Wirbelschleppenmodell mit den Ergebnissen der Simulationen verglichen. © 2001 Éditions scientifiques et médicales Elsevier SAS

Wirbelschleppe / stabile Schichtung / Turbulenz / kurzwellige Instabilität / kohärente Strukturen / numerische Simulation

* Correspondence and reprints.
E-mail address: frank.holzaepfel@dlr.de (F. Holzäpfel).

1. Introduction

The continuous increase of air traffic which increasingly congests airports due to their relative stagnation of capacities [32], on the one hand, and intentions to build super-large civil aircraft, on the other hand, have reinduced extensive wake vortex research in the last years. In spite of comprehensive previous research efforts, basic understanding of the influence of meteorological conditions on wake vortex physics still is quite controversial [29]. This may be due to the fact that wake vortices need large domains and high resolution in both simulation and experiment to be investigated properly. In both approaches, the Reynolds numbers which can be achieved are far from reality. On the other hand, in field experiments the meteorological conditions cannot be controlled or reproduced and are – as well as the wake vortices – difficult to measure in the required temporal and spatial resolution.

The impact of stable stratification on wake vortices has been discussed controversly for some years. Whereas some analyses show that wake vortices may accelerate their descent due to baroclinic effects [3,26] or may oscillate in a similar way as a displaced buoyant parcel of fluid [22] several investigations based on high-resolution 2D simulations [5,13,19,24,28] demonstrate that an early deceleration phase is followed by a subsequent acceleration. Similar results were achieved much earlier with a simple point vortex method [11]. Agreement with experiments [4,23,31] which indicate that the vortices decelerate and stop their descent after roughly $1/4$ of the oscillation period was obtained in early 2D simulations by fortune because the subsequent acceleration period was supressed by an overestimated diffusion [10,20]. Consensus seems to emerge from recent 3D simulations [4,6,21, 25,30] which corroborate our current results: during the early descent the wake vortices simultaneously decelerate and approach each other. A subsequent acceleration is not seen or is widely damped.

The recent 3D studies focus upon different aspects of the evolution of the trailing vortices: Schowalter et al. [25] performed a spatial large eddy simulation (LES) and concentrated on the initialization and development of the wake vortices as a function of time and space. In contrast to the 2D studies they did not find an acceleration phase, which they attribute to a modified distribution of the baroclinically produced vorticity [26]. Garten et al. [6] investigated the single-wavelength excited evolution of the Crow instability in ambient stratification, putting much effort on the vortex reconnection. In both works no turbulent fluctuations are initialized, and a symmetry boundary condition midway between the vortices is prescribed which inhibits vortex decay by turbulent vorticity transport across the boundary and the formation of asymmetric disturbances as the short-wave instability. Switzer and Proctor [30] initialized almost isotropic ambient turbulence on three different turbulence levels and state that depending on the degree of stratification and turbulence long and/or small-scale instabilities dominate the decay. Robins and Delisi [21] and Delisi and Robins [4] introduced turbulence by initializing their vortex pair as a superposition of many counter-rotating vortices with axes perturbed sinousoidally at different wavelengths and phases. They infer that the Crow instability is promoted by stable stratification and decelerates the descent compared to 2D simulations [21]. When perturbations are initialized on sufficiently small length scales they find that stratification causes a more rapid growth of short-wave instabilities at the expense of long-wave instabilities [4].

In our large eddy simulations we distinguish explicitly different sources of turbulence. Turbulence may stem from the aircraft or, additionally, from weak, anisotropic and decaying atmospheric turbulence. We first compare 2D and 3D results in terms of the temporal development of characteristic quantities such as descent height, vortex spacing and circulation. It is shown that the early development of the trailing vortices is not affected by the different turbulence scenarios. The following decay mechanisms, however, depend strongly on both the prescribed stratification and turbulence. The different mechanisms are discussed. Finally, results of Greene's approximate model [9] are compared to the simulated cases.

2. Numerical approach and parameters

Our code LESTUF is based on a Boussinesq large-eddy simulation code which uses the classical Smagorinsky closure and was originally developed to simulate turbulence under influence of constant background shear and stratification [16]. The code solves the discretized equations on a staggered grid with finite differences of second order accuracy in space and time. The discretization scheme is weakly diffusive and not dissipative. Meanwhile, LESTUF has proved its reliability in several wake vortex studies [7,8,13] in turbulent and stratified surroundings.

For most simulations we chose a domain size of $L_x \times L_y \times L_z = 408 \times 256 \times 540$ m^3 with a uniform grid of $\Delta y = \Delta z = 1$ m in spanwise, y, and vertical direction, z. In flight direction, $-x$, a resolution of $\Delta x = 6.375$ m was used. Periodic boundary conditions are employed in all three directions. The influence of neighbouring wakes results in the production of some artificial vorticity along the boundaries which is due to a small kink in the initial velocity distribution across the boundaries. The resulting disturbances are negligible since the boundaries are sufficiently far apart from the primary vortices. An effective Reynolds number, based on circulation and turbulent viscosity at core radius, of 7400 was achieved [8].

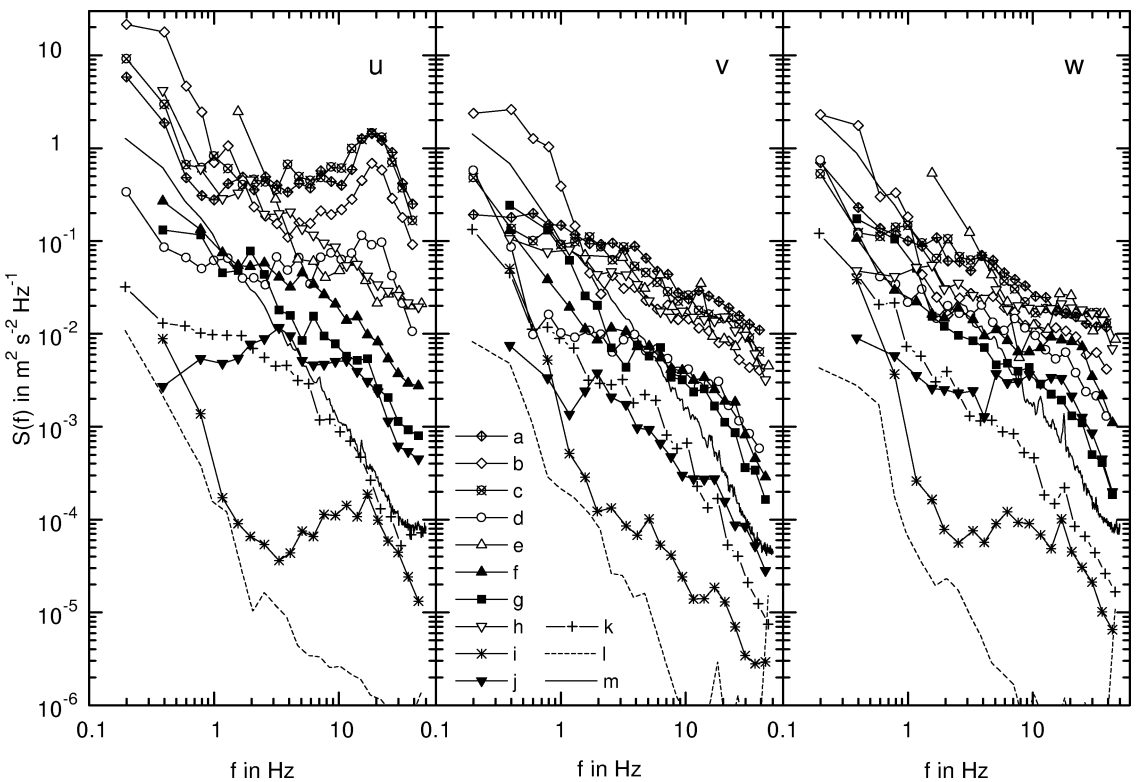

Figure 1. Power density spectra established from in-situ measurements behind different cruising aircraft and in free atmosphere. Open symbols denote near-field and closed symbols far-field data: (a) B737-300, $\Delta x = 43$–57 m, jet; (b) B737-300, $\Delta x = 40$–60 m, wake; (c) A340, short distance, jet; (d) A340, short distance, wake; (e) A310-300, $\Delta x = 100$–150 m; (f) A310-300, $\Delta x = 450$–600 m; (g) A310-300, $\Delta x = 800$ m; (h) VFW614, $\Delta x = 100$ m, center; (i) VFW614, $\Delta x = 80$ m, below; (j) VFW614, $\Delta x = 1.6$ km; (k) B727, $\Delta x = 15$ km; (l) free atmosphere, VFW614 case, $z = 8.2$ km; (m) convective boundary layer, $z = 1\,\text{km} \equiv 0.55 z_i$.

Two different approaches concerning the initialized turbulence were pursued. In case *(b)* the wake vortices develop in quiescent atmosphere; turbulence then only stems from the turbulent aircraft boundary layer, the mixing of the separated flows at the trailing edges, and the turbulent exhaust jets. Case *(b)* is a conservative approach which explores maximum life spans. From in-situ five-hole-probe velocity measurements performed with the DLR research aircraft FALCON chasing B737, A340, A310, B727, and VFW614 (ATTAS) aircraft in different distances, power density spectra were established (see *figure 1*) which reveal that the intensity of the aircraft induced turbulence may vary with several orders in magnitude. Maximum rms values of about 5.4 m/s (see *table I*) were found in the axial velocity component when the FALCON immerged into the exhaust jet region at small distances. Minimum rms values of 0.036 m/s were measured (curve (i)) at the lower edge of the downwash, in an airmass which was probably displaced by the downwash and did not directly experience aircraft-induced turbulence. Two spectra obtained from measurements in the undisturbed atmosphere are also included for comparison. The spectra of undisturbed air at high altitude show

Table I. Root mean square velocities determined by integration over spectra in *figure 1*. Frequencies below 1 Hz are excluded in integration to avoid adulterations caused by aircraft movements in the wake (cases (a)–(k)).

	u' [m/s]	v' [m/s]	w' [m/s]
(a)	5.4	1.1	1.0
(b)	3.6	0.76	0.7
(c)	5.5	0.94	1.0
(d)	1.5	0.35	0.51
(e)	2.4	0.88	1.3
(f)	0.76	0.35	0.53
(g)	0.52	0.35	0.33
(h)	1.6	0.79	0.91
(i)	0.057	0.036	0.047
(j)	0.35	0.12	0.28
(k)	0.19	0.14	0.13
(l)	0.05	0.06	0.04
(m)	0.77	0.81	0.94

significantly lower values than the data from the convective boundary layer [14]. It is noteworthy that the latter spectra are situated well within the aircraft-induced spectra. The distinct variations of the aircraft induced turbulence were taken into account in the simulations by adding initially a three-dimensional random pertubation field to the swirling flow such that the perturbations reach maximum rms values of 0.02 m/s, 0.2 m/s or 2 m/s at the core radius, r_c, and decay exponentially for smaller and larger radii. The best guess of 2 m/s was used as standard case *(b)*.

In case *(a)*, in addition to the aircraft-boundary layer turbulence, weak to moderate, anisotropic, and decaying atmospheric turbulence is superimposed on the whole velocity field. The atmospheric turbulence which is described in detail in [8] obeys prescribed spectra with rms velocities of 0.38 m/s in horizontal and 0.21 m/s in vertical direction. The length scales of the most energetic eddies amount to 60–90 m and local maximum velocities to approximately ±1.4 m/s. The resulting dissipation rate is $\varepsilon = 3.2 \cdot 10^{-5}\,\mathrm{m^2/s^3}$.

The wake vortices were initialized as superposition of two Lamb–Oseen vortices where the tangential velocity profile of one vortex is given by

$$v_t(r) = \frac{\Gamma_0}{2\pi r}\left(1 - \exp\frac{-r^2}{r_0^2}\right), \quad r_0 = \frac{r_c}{1.121} \qquad (1)$$

with a core radius of $r_c = 4$ m. A root-circulation of $\Gamma_0 = 565\,\mathrm{m^2/s}$ and a vortex spacing of $b_0 = 47$ m were employed to represent the cruising B-747 aircraft with an elliptical wing loading. In contrast to the single Lamb–Oseen vortex the superposition of two vortices is not a particular solution of the Navier–Stokes equations. A transient self-adaption phase to a dipole family which is a quasi-steady solution of the Euler equations may introduce additional perturbances to the flow [27]. However, Sipp et al. [27] show that for our small ratio $r_{c0}/b_0 = 0.085$ the distortions are weak.

The mean potential temperature gradient of the atmosphere, $\mathrm{d}\Theta/\mathrm{d}z$, was constant in each calculation and the corresponding Brunt–Väisälä frequency

$$N = \left(\frac{g}{\Theta_0}\frac{\mathrm{d}\Theta}{\mathrm{d}z}\right)^{1/2} \qquad (2)$$

varied between 0 and 0.056/s ($\mathrm{d}\Theta/\mathrm{d}z = 0$–$10\,\mathrm{K}/100$ m). Since our previous 2D investigations [13] showed that the prominent phenomena are only intensified by increasing the stratification from $N = 0.01$/s to $N = 0.04$/s but do not change in principle, we consider here two benchmark cases with $N = 0.014$/s and $N = 0.04$/s. However, in 2D the vortex behaviour is categorically modified for even higher stratification such that the vortices rise to the flight path. Therefore, the case $N = 0.056$/s is also included in the current study to see whether this hazardous scenario is likely to occur in 3D.

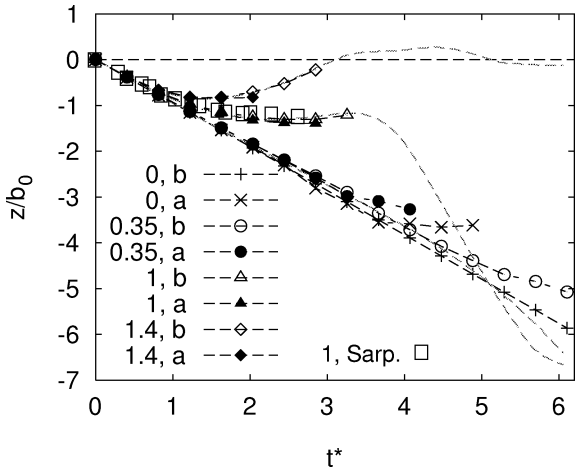

Figure 2. Normalized descent distance versus time for different turbulence scenarios (*(b), (a)*) and Brunt–Väisälä frequencies, $N^* = 0, 0.35, 1, 1.4$. Grey dashed curves denote 2D simulations [13]. Squares are Sarpkaya's experimental data [23].

3. Results and discussion

Most results are presented in non-dimensionalized form. The characteristic scales are based on the initial vortex separation, b_0, and circulation, Γ_0, leading to the time scale

$$t' = \frac{2\pi {b_0}^2}{\Gamma_0} = \frac{b_0}{w_0} = 24.6\,\mathrm{s}, \qquad (3)$$

where w_0 is the initial descent speed of the vortex pair. For the normalized time and Brunt–Väisälä frequency it follows $t^* = t/t'$ and $N^* = Nt'$, respectively. This means that the Brunt–Väisälä frequencies investigated are $N^* = 0, 0.35, 1.0$, and 1.4. The inverse of N^* corresponds to the vortex Froude number. The normalized eddy dissipation rate in case *(a)* is $\varepsilon^* = (\varepsilon b_0)^{1/3}/w_0 = 0.06$.

3.1. Descent height and vortex spacing

Figure 2 depicts the temporal development of the normalized descent height[†], z/b_0. Results of 2D simulations without any turbulence [13] (grey dashed lines) are also included. We observe that for early times ($t^* < 1$) neither stratification nor turbulence alter the descent of the vortex pair. Later on, however, it is clearly seen that the level of stratification controls the decelerated descent; the introduction of turbulence and changes of the type

[†] The vortex centers were determined by searching the local minima of the second eigenvalue λ_2 of the symmetric tensor $S^2 + \Omega^2$ which is a measure for coherent vortex structures [15]. S and Ω are the symmetric and antisymmetric parts of the velocity gradient tensor ∇u.

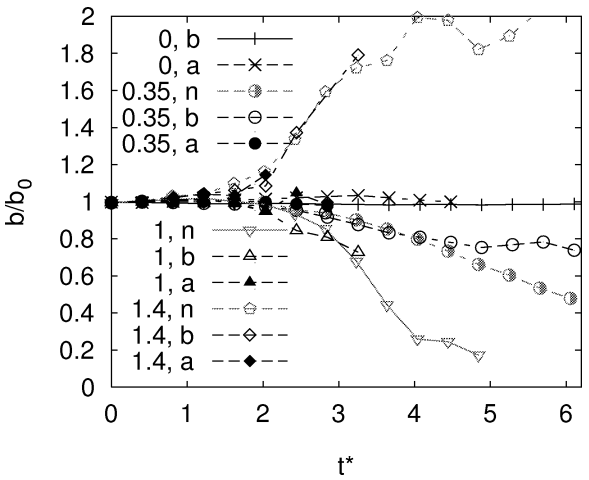

Figure 3. Normalized vortex spacing versus time for different turbulence scenarios (*(n), (b), (a)*) and Brunt–Väisälä frequencies, $N^* = 0, 0.35, 1, 1.4$. Cases *n* denote no turbulence.

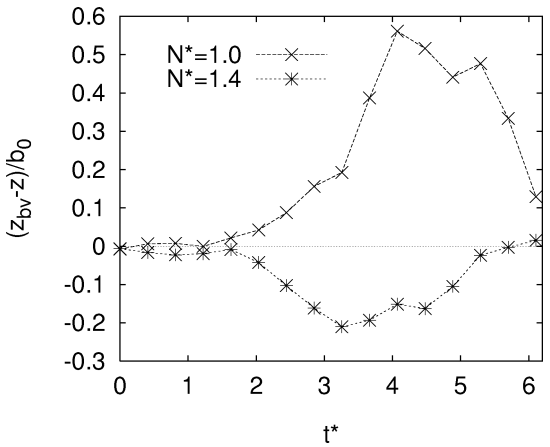

Figure 4. Normalized vertical offset between centroid of BV and vortex core position for two different stratifications.

of turbulence (*(b)* or *(a)*) only alter this behaviour marginally. The late acceleration of descent, which is seen for moderate to strong stratification in 2D, cannot be identified in the turbulent cases. The trajectories cease earlier with turbulence when they cannot be determined uniquely because of advanced vortex destruction (see below). In general the lifespan is shorter, the higher the stratification for a given turbulence (and, vice versa, the higher the degree of initial turbulence for a given stratification). In the neutral and quiescent atmosphere (case *b* with $N^* = 0$), the descent continues beyond times of $t^* = 12$ and reaches altitudes below $z/b_0 = -10$ (not shown). In contrast to that, *figure 2* demonstrates that either weak stratification (case *(b)* with $N^* = 0.35$) or weak atmospheric turbulence (case *(a)* with $N^* = 0$) is sufficient to reduce the longevity of wake vortices considerably. For $N^* = 1.4$, the 2D simulations show that the vortices may rebound to the glide path. The same rebound is observed if boundary-layer turbulence is superimposed (case *(b)*). However, the vortices then lose identity after $t^* = 3$; if also (even weak) atmospheric turbulence is present, the process of erosion is faster ($t^* = 2$) such that no coherent piece of vortex is observed to rebound. Note that the simulations also agree well with Sarpkaya's towing tank experiments [23] for $N^* = 1$.

The major trends of the temporal evolution of the vortex spacing, b/b_0 (see *figure 3*), are also independent of the prescribed turbulence for a given stratification. The spacing remains constant for neutral stratification. For stratifications increased up to $N^* = 1$ the vortices start to approach each other after $t^* \approx 2$. Minor deviations of the vortex spacing at identical stratification levels indicate spatial deformation of the vortex lines by turbulence. For $N^* = 1.4$, the vortex spacing increases with time.

We conclude that the agreement between turbulent and laminar cases regarding vortex descent and vortex spacing clearly indicates that the underlying physics of the early development is intrinsically two-dimensional. The observations that the vortices approach each other for $N^* \leqslant 1$ and, at the same time, decelerate (which is seemingly a contradiction regarding the concept of mutual velocity induction) can be fully explained when analyzing the flows induced by primary and counter-rotating baroclinic vorticity (BV) (cf. Figs. 7, 9, 10 in [13]). The BV is produced along the border of the adiabatically heated vortex oval by the baroclinic torque [26] according to

$$\frac{\mathrm{D}\omega}{\mathrm{D}t} \sim \frac{1}{\rho^2}\nabla\rho \times \nabla p. \tag{4}$$

The BV, which grows and accumulates along the separating streamline from bottom to top when the vortex pair is descending through stably stratified air, induces an upward and inward motion on the vortex oval. The upward motion weakens the primary descent speed, the approaching vortices decelerate. On the other hand, when $N^* = 1.4$, the BV-induced upward velocity dominates the descent speed and the oval starts to rebound at $t^* = 1.6$ (see *figure 2*). Now BV accumulates from top to bottom along the separating streamline. It still induces an upward but now outward flow on the oval and, hence, the vortices rise quicker and separate. This behaviour can be better understood when analyzing the vertical offset between the vortex center and the centroid of the BV. Comparing *figures 3* and *4* we see that the vortices separate (approach) when the centroid of BV is situated below (above) the vortex cores. (For $N^* = 1.4$ the effect of vortex separation is additionally intensified by local BV production which is stronger at the lower part of the oval due to the strong vertical temperature gradient.) We explain the different time delays for the onset of the deceleration (*figure 2*) and for the onset of

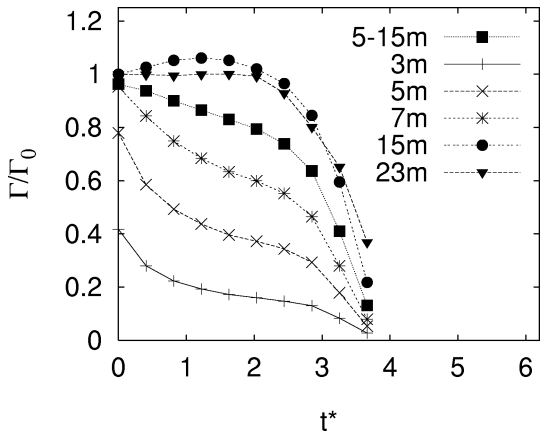

Figure 5. Case *(a)*, $N^* = 0.35$. Normalized circulation versus time computed over circles with different radii 3 m to 23 m; normalized circulation averaged over radii from 5 m to 15 m.

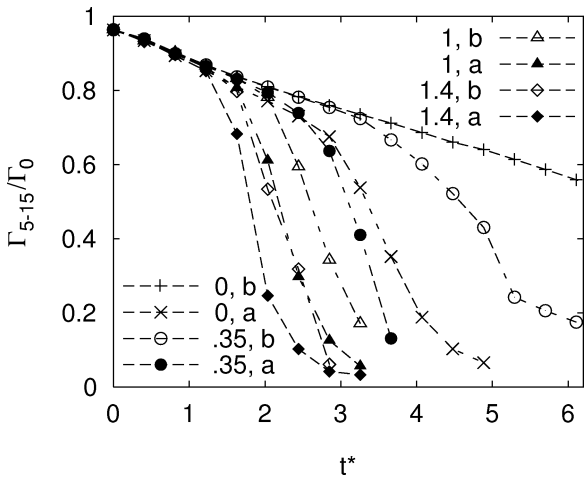

Figure 6. Normalized circulation averaged over circles with radii from 5 m to 15 m versus time.

the change of vortex spacing as follows: about 1 t' is necessary to produce BV sufficient for the retardation of the oval; additional 0.5 to 1 t' is required to establish the vertical offset between BV centroid and vortex center by advection.

3.2. Circulation

Figure 5 displays examplarily for case *(a)* with $N^* = 0.35$, the decay of circulation computed over different radii. For times up to $t^* = 2.5$ an exponential type decay is observed on small and intermediate radii which is due to internal diffusion (core radius growth). Maximum circulation is found at $r = 15$ m because at larger radii the integration area also encloses some BV which reduces Γ/Γ_0. After $t^* = 2.5$ – the beginning of the subsequent rapid decay – the BV is in part detrained such that maximum circulation values are found at $r = 23\,\text{m} \approx b_0/2$. In the following we use a circulation Γ_{5-15} which is averaged over circles with radii from 5 m to 15 m. ‡

Figure 6 shows that the initial decay is identical for all cases. Then, the individual curves detach from the bunch of curves at different times to initiate a phase of rapid decay. The higher the turbulence level and the stronger the stratification the earlier the final decay of circulation starts. Different turbulence scenarios only play a significant role for the onset of rapid decay when stratification is neutral to weakly stable ($N^* = 0, 0.35$). Generally we note that in all our scenarios, except for the unlikely case of zero stratification and no ambient turbulence, the circulation always drops to values below 20% of the initial strength within $6t'$ which is less than 2.5 minutes.

It is noteworthy that at the time when the vortices have rebounded to 10 m below the glide path (case *(b)*, $N^* = 1.4$), the circulation has reduced already to 5% of its initial value. Hence, from this and from the trajectory discussion above, we learn that the vortex rebound expected at very strong stratification (strong inversion layers), which is suspected to be very hazardous from an operational point of view, is probably harmless because of the advanced erosion of vortex coherence and strength.

3.3. Variation of aircraft-induced turbulence

Two further simulations were performed for case *(b)* with $N^* = 0.35$ where the initialized maximum rms turbulence values were reduced from 2 m/s to 0.2 m/s and 0.02 m/s. These variations over two orders of magnitude were carried out to take into account the uncertainty concerning realistic aircraft boundary-layer turbulence levels, to check the sensitivity to the prescribed turbulence, and, particularly, to conservatively explore maximum lifespans of wake vortices in stably stratified environments. *Figure 7* indicates that, when changing the aircraft-induced turbulence by two orders of magnitude, the descent height remains unaffected until $t^* = 4.5$ and differs by one initial vortex spacing only at $t^* = 6$. From *figure 8* we learn that factor of 10 stronger aircraft turbulence leads only to a time shift for onset of rapid decay of less than $\Delta t^* = 0.8$. At $t^* = 6$ the circulation of all vortices is reduced to about 20% of the initial value. These facts overall indicate a minor sensitivity of the underlying decay mechanism on the strength of the boundary-layer perturbations and show that the cases *(b)* can be read as

‡ Such a definition is especially appropriate when numerical predictions are to be compared to field measurements due to several reasons: Only intermediate radii are reliably accessible by LIDAR; some averaging of data is included which reduces its scatter; measurement errors due to the neighbouring vortex are less sensitive to the viewing angle [1]; and Γ_{5-15} correlates well to effects of wake encounters [12].

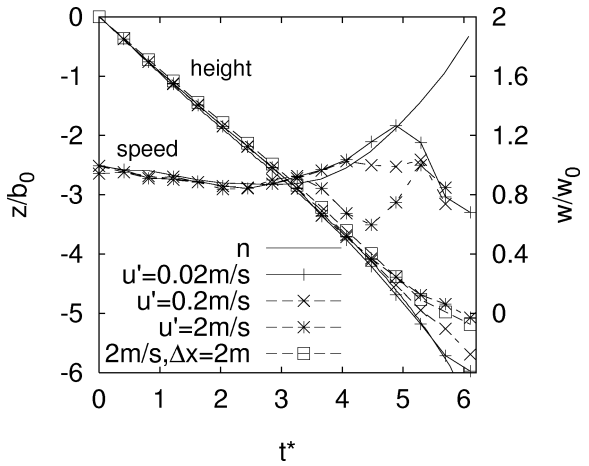

Figure 7. Descent height (left ordinate) and speed (right ordinate) versus time for different initial levels of aircraft induced turbulence and one case with increased axial resolution, $N^* = 0.35$.

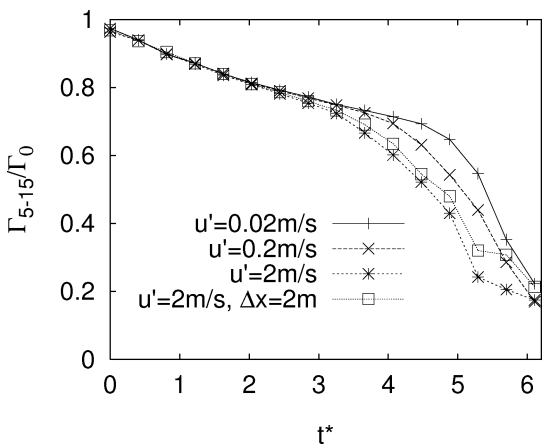

Figure 8. Γ_{5-15}/Γ_0 versus time for different prescribed levels of aircraft turbulence and one case with increased axial resolution, $N^* = 0.35$.

conservative estimates of the lifespan of wake vortices in a stably stratified atmosphere.

Moreover, in *figure 7* the descent speed, w/w_0, once again elucidates the sequence of the 2D/3D behaviour. All wakes follow, at least to a certain extent, the de-accelerated descent of the 2D simulation until the phase of 3D vortex destruction (see *figure 8*) commences. The acceleration occurs when the induced descent speed, which is increased due to the vortex approach, dominates the deceleration caused by BV. To our knowledge only one experimental work [31] reports weak acceleration.

3.4. Structural development

The development of the vortex structure during decay is depicted in *figure 9* for case *(b)* without stratification

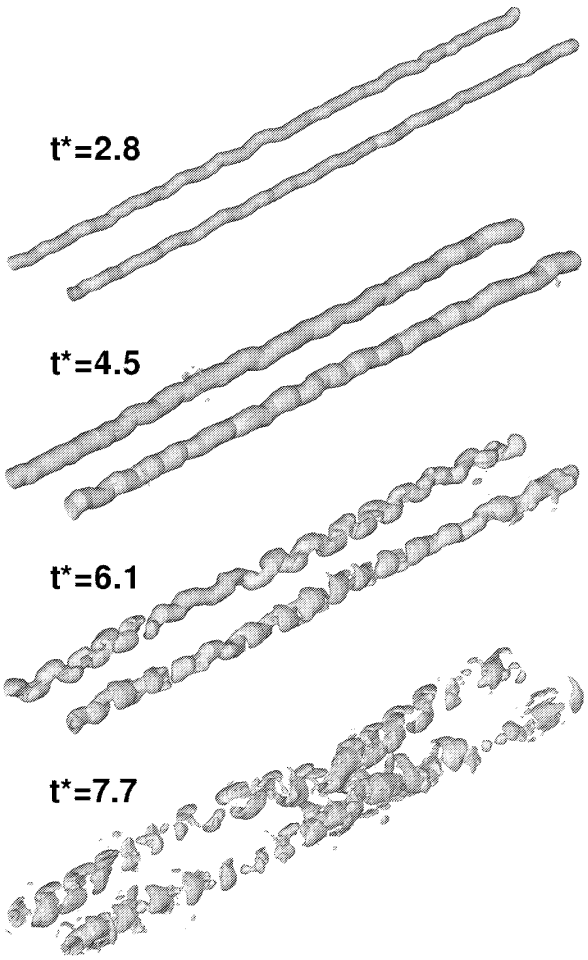

Figure 9. Perspective view of λ_2^*-surfaces for case *b*, $N^* = 0$; $\lambda_2^*(t^* = 2.8) = -3000$, others: $\lambda_2^* = -1200$.

in normalized λ_2-surfaces (see footnote in section 3.1) for several instants of time. At $t^* = 2.8$ pertubations can be identified which resemble the early stages of the development of the short-wave instability [33]. Indeed, the phase relation (in-phase in horizontal view and out-of-phase in side view) and the wave length of $\lambda \approx 4r_c$ correspond roughly to the characteristics observed in the short-wave or so-called cooperative elliptic instability [17,18]. Since the axial resolution of the simulations was not sufficient to properly resolve the short-wave instability, the amplitude of the instability is somewhat modulated along the vortex axes. With advancing time the short-wave amplitudes are growing. Finally, at $t^* = 7.7$ the formation of the Crow instability [2] becomes evident.

With weak stratification, $N^* = 0.35$, the structural development shown in *figure 10* is distinctly modified. Although at $t^* = 2.8$ the wake vortices still look almost identical for weak and neutral stratification, the subsequent growth rates of the short-wave and the long-wave

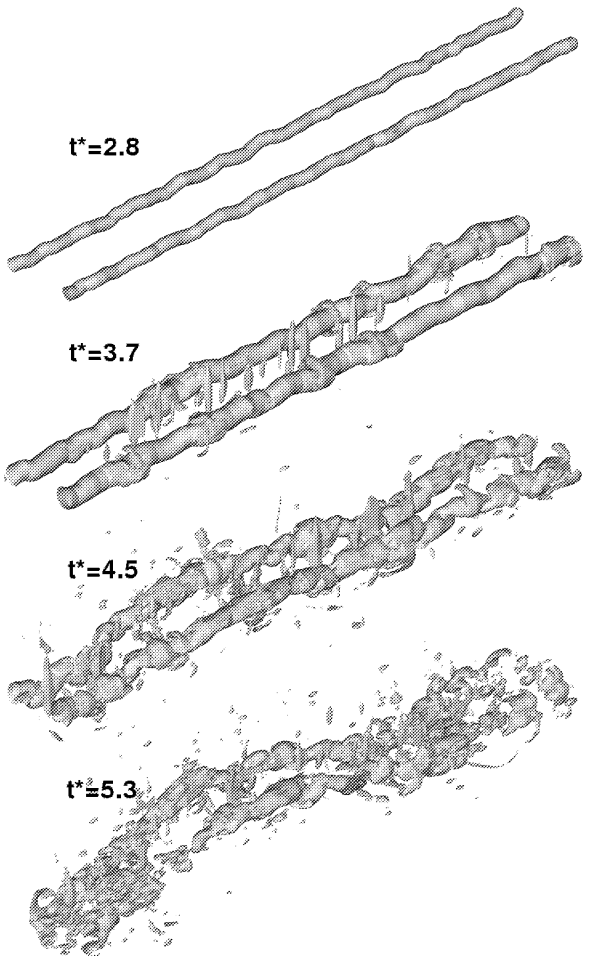

Figure 10. Perspective view of λ_2^*-surfaces for case *b*, $N^* = 0.35$; $\lambda_2^*(t^* = 2.8) = -3000$, others: $\lambda_2^* = -1200$.

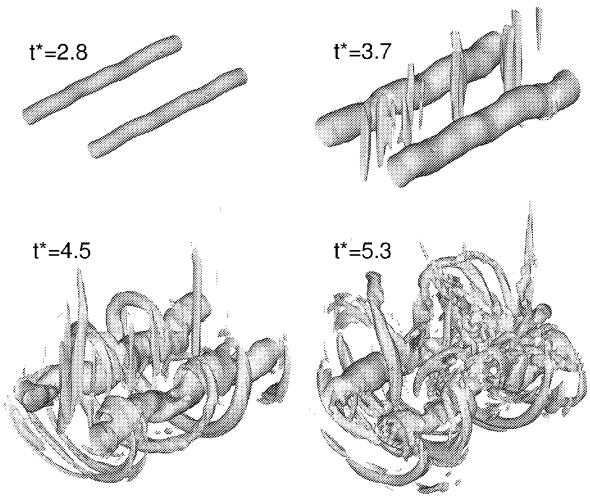

Figure 11. As *figure 10* with increased axial resolution ($\Delta x = 2$ m) in an axially shortened domain.

amplitudes are substantially larger for the stratified case (compare stages at $t^* = 4.5$). This is possibly due to the reduction of the vortex spacing for $t^* > 2$ (see *figure 3*) which sustains amplification of short-wave instabilities. Furthermore, at $t^* = 3.7$ vertical λ_2^*-streaks between the vortices (also seen in [4]) become visible which play – as we will show below – a crucial role regarding the accelerated decay. The vertical streaks, ultimately, produce turbulence which explains the less clear formation of the short-wave structures. For simulations with reduced levels of aircraft turbulence we find that the λ_2^*-surfaces are smoother such that the short-wave instability is seen somewhat more clearly. The overall decay is delayed and the long-wave (Crow) instability is less obvious (not shown).

Case *(b)*, $N^* = 0.35$ was repeated with an increased axial resolution of $\Delta x = 2$ m in an axially reduced domain of $L_x = 96$ m to ensure that our investigations are meaningful in spite of the insufficient resolution of the short-wave disturbances. *Figures 7* and *8* indicate that the most important parameters, descent height and circulation decay, are almost identically reproduced. The somewhat delayed decay for $t^* > 4$ may be due to the exclusion of the Crow instability in the short domain. The comparison of the structural development in *figures 10* and *11* underlines the similarity of the evolution until $t^* = 3.7$. With finer resolution, sure enough, the short-wave oscillation is better resolved but the vertical structures at $t^* = 3.7$ occur likewise. Considering the deformation of the vortices later, a distinct similarity still persists. However, the noticeable azimuthal structures are obviously less coherent in the coarser grid. Regarding the similarity of the statistical results in *figures 7* and *8*, such coherence does not seem to play a major role in the decay process.

For strong stratification ($N^* = 1$), short-wave perturbations develop even faster (compare *figure 12(a)* at $t^* = 2.4$ with *figure 10* at $t^* = 2.8$ and 3.7), and the shape is even more disturbed. *Figure 12(b)*, showing a higher λ_2^*-value at the same time, indicates that the production of the azimuthal BV structures ('ribs') is modulated already by small short-wave pertubations. This induces strong vortical structures along the mid plane between the vortices which in turn trigger the rapid decay. Crow instability is not evident in cases *(b)* for strong stratification, $N^* \geqslant 1$. The promotion of short-wave instabilities at the expense of long-wave instabilities for strong stratifications is also reported in an experimental and numerical study [4].

In the cases *(a)* (with weak and decaying atmospheric turbulence, *figures 13, 14*), we find phenomenologically very similar developments for all investigated stratifications. However, with atmospheric turbulence as well as stronger stratification the vortices decay quicker. As

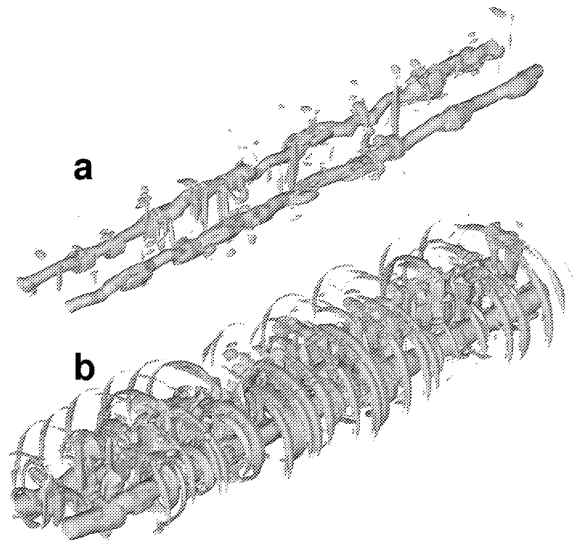

Figure 12. Perspective view of λ_2^*-surfaces for case *(b)*, $N^* = 1$ at $t^* = 2.4$: (a) $\lambda_2^* = -3000$, (b) $\lambda_2^* = -600$.

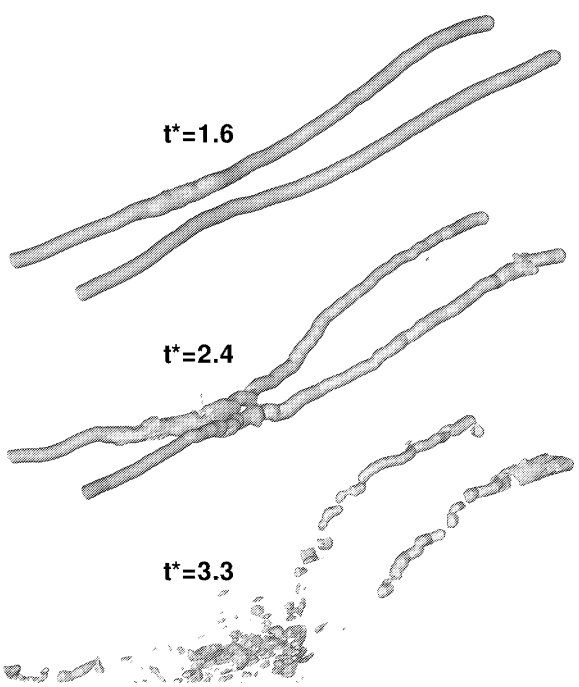

Figure 13. Perspective view of λ_2^*-surfaces for case *(a)*, $N^* = 0.35$, $\lambda_2^* = -3000$.

Robins and Delisi [21], and, later in a more refined consideration, Garten et al. [6] pointed out, the approach of the vortices caused by BV and the perturbation growth due to the Crow instability combine to accelerate the coming together of portions of the vortices. This can be seen by comparing *figures 13* and *14* for $t^* = 1.6$. Later,

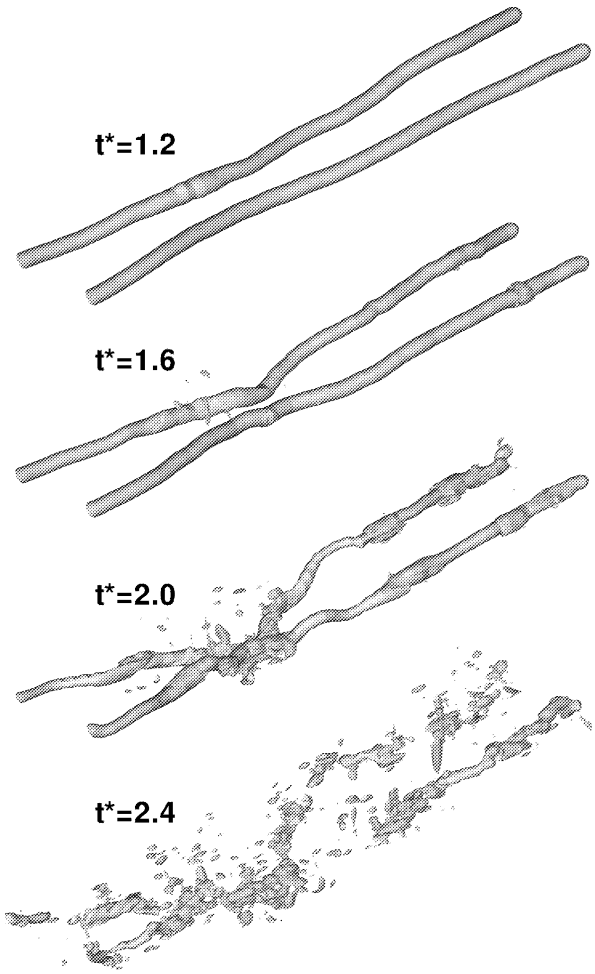

Figure 14. Perspective view of λ_2^*-surfaces for case *(a)*, $N^* = 1$, $\lambda_2^* = -3000$.

the final destruction originates from the portions were the vortices link first. Short-wave disturbances show up where separation is minimum (*figure 13* for $t^* = 2.4$) and then spread out rapidly along the vortices. This is in contrast to other results [6,21] where the formation of longer living descending vortex rings is observed. We thus argue that the interference of BV structures with short-wave disturbances leads to the rapid destruction as known from case *(b)*. The short-wave disturbances are forced by small-scale turbulence from the aircraft-boundary layer and are absent in the other studies. The accelerated decay as a result of interaction of short-wave and long-wave instabilities was demonstrated experimentally ([18], their section 5).

3.5. Decay mechanism

In order to explain the decay mechanisms observed in our simulations we show *figures 15*, *16* and *17* which

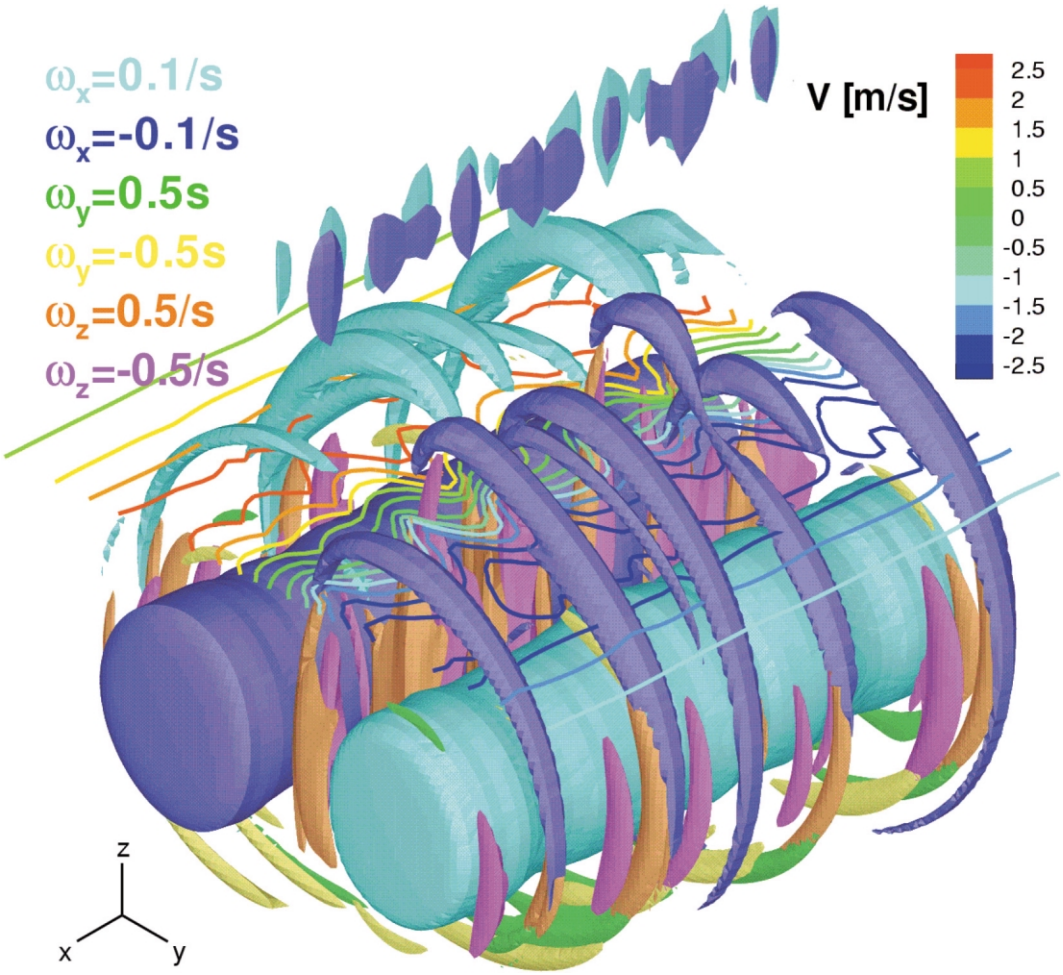

Figure 15. Iso-surfaces of all three vorticity components in a perspective view and iso-lines for lateral velocity v in a horizontal plane above the vortices. Case *(b)*, $N^* = 0.35$, $t^* = 2.8$, high axial resolution.

display iso-surfaces of all three vorticity components at $t^* = 2.8$ in perspective, top, and front view, respectively, for case *(b)*, $N^* = 0.35$, and high axial resolution (see *figure 11* for the corresponding λ_2^*-surfaces). Above the vortices a horizontal plane with iso-lines for the lateral velocity component, v, is included ('v-plane'). The top-view elucidates that the rib-like structures of baroclinically produced ω_x induce below lateral velocities, v, which are directed towards the symmetry plane between the vortices. The induced wavy velocity field exhibits steep axial gradients of the lateral velocity, $\partial v/\partial x$, and, equivalently, vertical vorticity, $\omega_z \sim \partial v/\partial x$. In detail, each 'BV-rib' induces a tongue-like structure which is flanked by the origin of a pair of counter-rotating vorticity streaks, ω_z. This vorticity is then strongly stretched by the accelerating downward motion between the main vortices yielding very intense ω_z-streaks (note that the iso-surface of ω_z has a five times higher magnitude than ω_x). Assuming stationarity, vortex stretching changes vorticity according to

$$\frac{\mathrm{D}\omega_z}{\mathrm{D}t} = w\frac{\partial \omega_z}{\partial z} = \omega_z \frac{\partial w}{\partial z}. \tag{5}$$

The integration from a position 0 midway between the vortices in the 'v-plane' to a vertical position 1 between the vortex centers gives

$$\int_0^1 \frac{\partial}{\partial z}(\ln \omega_z)\,\mathrm{d}z = \int_0^1 \frac{\partial}{\partial z}(\ln w)\,\mathrm{d}z, \tag{6}$$

which leads to

$$\frac{\omega_{z1}}{\omega_{z0}} = \frac{w_1}{w_0}. \tag{7}$$

From vertical positions 0 to 1 the downwards directed velocity increases from $w_0 \approx -0.3\,\mathrm{m/s}$ to $w_1 \approx -6\,\mathrm{m/s}$

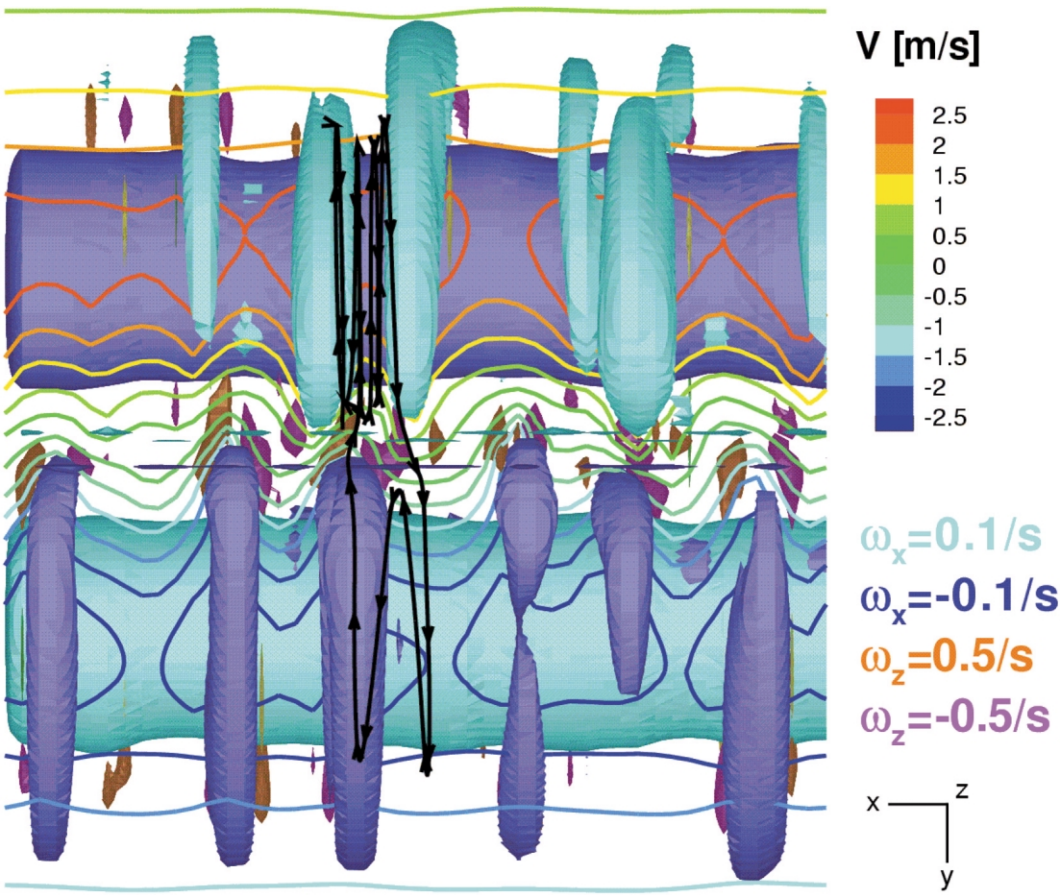

Figure 16. Top view of *figure 15*. The black streamline indicates transport across the symmetry plane.

which yields an intensification of ω_z by a factor of $\omega_{z1}/\omega_{z0} = w_1/w_0 = 20$. Below the main vortex centers, ω_z is reduced by vortex broadening which is caused by the deceleration experienced during advection towards the lower stagnation point (*figure 17*). Then, the vorticity is tilted, and becomes visible again after another acceleration first in the lateral, ω_y, and then again in the vertical vorticity component, ω_z. The central vertical streaks acting like counter-rotating rolls are outmost effective in exchanging fluid between the two vortices. This is demonstrated by a streamline which crosses the symmetry plane twice (*figures 16, 17*). Aside from a general strong turbulence production caused by counter-rotating vortices in the whole oval, the coherent lateral exchange of fluid across the centerline enables the rapid turbulent diffusion of primary vorticity from one side to the other. This effect is prerequisite for the rapid turbulent decay of vortex pairs. We found that similar mechanisms which comprise the steepening of $\partial v/\partial x$ and vortex stretching are also responsable for the rapid decay observed in weak to moderate atmospheric turbulence (not shown).

3.6. Parameterized model

Here, we apply Greene's approximate model [9] (GM) to the simulated cases. In GM the impulse of the aircraft wake, $I_0 = \rho_0 b_0 \Gamma_0$, is reduced by the sum of three forces comprising a viscous force, a turbulence force, and the buoyancy force. The constants in the viscous term and the turbulence term are set to $C_D = 0.2$ and to 0.41, respectively.

Figure 18 shows that in case *(a)* satisfactory agreement is achieved regarding the descent. Similar deviations – underestimation of the descent for weak stratification and overestimation for very strong stratification – are also found in cases *(b)*. However, for strong stratification (see *figure 19*) GM predicts zero circulation when Γ_{5-15}/Γ_0 is merely reduced to 0.5. The agreement of GM with the development of the circulation integrated over the halfplane indicates that GM assumes implicitly that the primary vorticity and the BV cancel each other immediately. However, the LES predicts well the separated vorticity for time spans during which the hazard of the vortices is underestimated by the simple model.

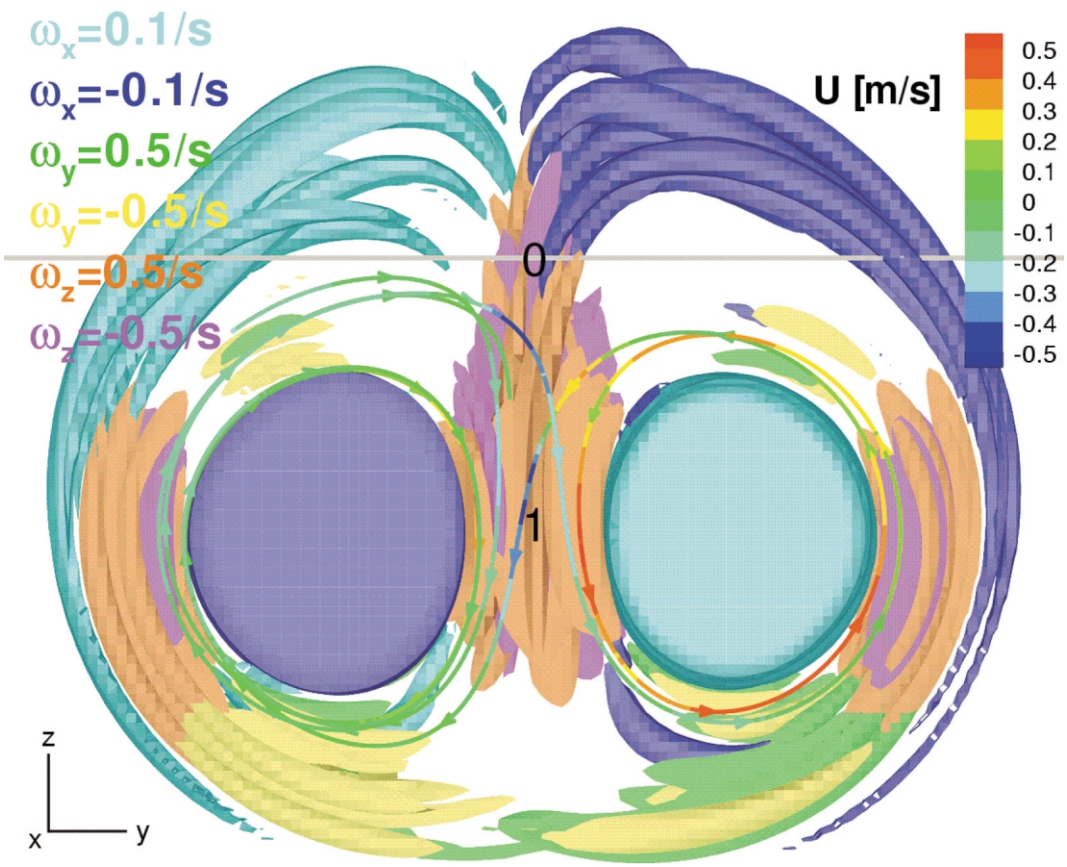

Figure 17. Front view of *figure 15*. Here the streamline is colour-coded according to its axial velocity u. The vertical position of the plane which shows lateral velocities in *figures 15, 16* is marked by grey line.

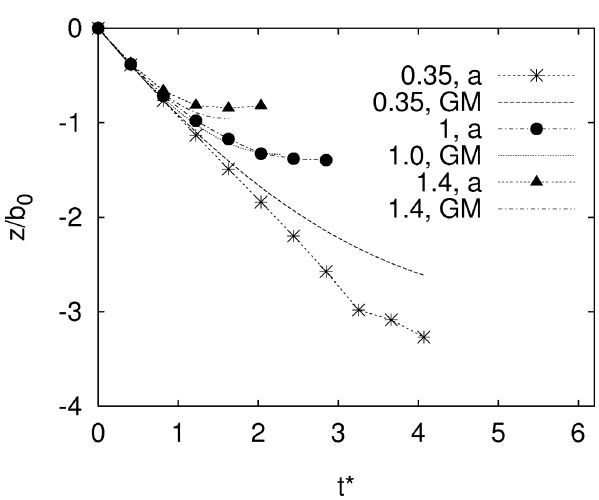

Figure 18. Comparison of normalized descent distance versus time between predictions of LES and Greene's model for atmospheric turbulence.

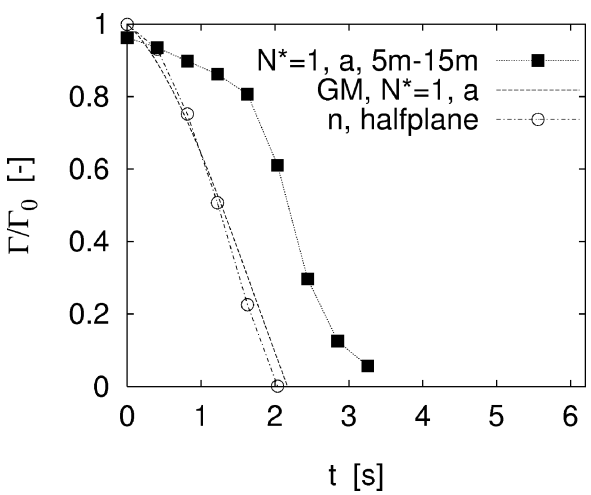

Figure 19. Case *(a)*, $N^* = 1$. Comparison of Γ_{5-15}/Γ_0 to normalized circulation of Greene's model. Furthermore, circulation determined by integration over one halfplane for case n.

4. Conclusions

We have performed LES of wake vortices in a stably stratified atmosphere with which we aim at more realistic conditions compared to previous 3D work [4,6,21,25,30]: we used a relatively high effective Reynolds number, initialized the vortices with relatively tight vortex cores, superimposed aircraft induced turbulence, and considered weak atmospheric turbulence.

The simulations elucidate that the early development of the wake vortices is only affected by the degree of stratification, and not by different turbulence scenarios as prescribed in our study. Descent speed, vortex spacing, and circulation develop almost identically for constant stratification – and can be described in a two-dimensional framework – until different destruction mechanisms initiate a phase of final decay.

Aircraft induced turbulence triggers short-wave instability modes. Owing to those disturbances, the baroclinically produced vorticity rearranges in rib-like structures which induce counter-rotating vertical vorticity-streaks between the primary vortices. These vorticity-streaks are substantially intensified by vortex stretching, and wrap around the main vortices. This results in rapid turbulence production inside the oval, and, in particular, represents an efficient exchange mechanism of primary vorticity across the center plane which leads to rapid circulation decay. Hence, in a calm atmosphere, it is the interaction of primarily independent processes (short-wave instability and baroclinic vorticity production) which initiates the quick dissolution of coherence and decay of circulation of the main vortices. In some cases at later stages also the long-wave (Crow) instability is established. Furthermore, the variation of the intensity of aircraft induced turbulence in a quiescent atmosphere allowed for the conservative estimation that stable stratification reduces the longevity of wake vortices considerably.

When in addition also weak and decaying atmospheric turbulence is prescribed, the sequence of dominant instability processes is reversed: first the Crow instability develops and short-wave disturbances accelerate the decay when the vortices link and thus suppress the formation of descending vortex rings. When atmospheric turbulence is present, the vortices decay sooner for a given level of stratification.

In a very strongly stratified and quiescent atmosphere, wake vortices may rebound to the flight level. This very hazardous scenario from an operational point of view is probably harmless because the vortices quickly lose almost all of their intensity during ascent.

Finally, it is shown that Greene's approximate model successfully predicts the vortex descent. However, the model overestimates the decay of circulation because it assumes intrinsically that main and baroclinically produced vorticity of opposite sign cancel each other immediately which, according to our LES, is only partially the case at late times.

Acknowledgements

This work was supported by the European Commission in the frame of the Brite/EuRam project WAVENC (No. BE97-4112).

References

[1] Campbell S.D., Dasey T.J., Freehart R.E., Heinrichs R.M., Matthews M.P., Perras G.H., Rowe G.S., Wake Vortex Field Measurement Program at Memphis, TN Data Guide, Project Report NASA/L-2, Lincoln Laboratory, Massachusetts Institute of Technology, 1997.

[2] Crow S.C., Stability theory for a pair of trailing vortices, AIAA J. 8 (1970) 2172–2179.

[3] Crow S.C., Motion of a vortex pair in a stably stratified fluid, Poseidon Research Rep. 1, Santa Monica, CA, 1974.

[4] Delisi D.P., Robins R.E., Short-scale instabilities in trailing wake vortices in a stratified fluid, AIAA J. 38 (2000) 1916–1923.

[5] Garten J.F., Arendt S., Fritts D.C., Werne J., Dynamics of counter-rotating vortex pairs in stratified and sheared environments, J. Fluid Mech. 361 (1998) 189–236.

[6] Garten J.F., Werne J., Fritts D.C., Arendt S., Direct numerical simulations of the Crow instability and subsequent vortex reconnection in a stratified fluid, subm. to J. Fluid Mech.

[7] Gerz T., Ehret T., Wingtip vortices and exhaust jets during the jet regime of aircraft wakes, Aerosp. Sci. Technol. 1 (1997) 463–474.

[8] Gerz T., Holzäpfel F., Wingtip vortices, turbulence, and the distribution of emissions, AIAA J. 37 (1999) 1270–1276.

[9] Greene G.C., An approximate model of vortex decay in the atmosphere, J. Aircraft 23 (1986) 566–573.

[10] Hecht A.M., Bilanin A.J., Hirsh J.E., Turbulent trailing vortices in stratified fluids, AIAA J. 19 (1981) 691–698.

[11] Hill F.M., A numerical study of the descent of a vortex pair in a stably stratified atmosphere, J. Fluid Mech. 71 (1975) 1–13.

[12] Hinton D.A., Tatnall C.R., A Candidate Wake Vortex Strength Definition for Application to the NASA Aircraft Vortex Spacing System (AVOSS), NASA Technical Memorandum 110343, Langley Research Center, Hampton, Virginia, 1997.

[13] Holzäpfel F., Gerz T., Two-dimensional wake vortex physics in the stably stratified atmosphere, Aerosp. Sci. Technol. 3 (1999) 261–270.

[14] Holzäpfel F., Gerz T., Frech M., Dörnbrack A., Wake Vortices in a Convective Boundary Layer and their Influence on Following Aircraft, J. Aircraft 37 (2000) 1001–1007.

[15] Jeong J., Hussain F., On the identification of a vortex, J. Fluid Mech. 285 (1995) 69–94.

[16] Kaltenbach H.-J., Gerz T., Schumann U., Large-eddy simulation of homogeneous turbulence and diffusion in stably stratified shear flow, J. Fluid Mech. 280 (1994) 1–40.

[17] Laporte F., Darracq D., Corjon A., On the Vortex-Turbulence Interaction: DNS of Elliptic Instability of a Vortex Pair, AIAA Paper 99-3417 (1999).

[18] Leweke T., Williamson C.H.K., Cooperative elliptice instability of a vortex pair, J. Fluid Mech. 360 (1998) 85–119.

[19] Pavlenko A.A., Influence of the Calm Atmosphere Stratification on the Evolution of the Vortex Behind an Aircraft, ISTC Moscow, Annual Report, Project No. 201-95 (1996) 33–40.

[20] Robins R.E., Delisi D.P., Numerical study of vertical shear and stratification effects on the evolution of a vortex pair, AIAA J. 28 (1990) 661–669.

[21] Robins R.E., Delisi D.P., Numerical simulation of three-dimensional trailing vortex evolution in stratified fluid, AIAA J. 3 (1998) 981–985.

[22] Saffman P.G., The motion of a vortex pair in a stratified atmosphere, SIAM LI (1972) 107–119.

[23] Sarpkaya T., Trailing vortices in homogeneous and density-stratified media, J. Fluid Mech. 136 (1983) 85–109.

[24] Schilling V., Siano S., Etling D., Dispersion of aircraft emissions due to wake vortices in stratified shear flows: A two-dimensional numerical study, J. Geophys. Res. 101 (1996) 20965–20974.

[25] Schowalter D.G., DeCroix D.S., Switzer G.F., Lin Y.-L., Arya S.P., Toward Three-Dimensional Modeling of a Wake Vortex Pair in the Turbulent Planetary Boundary Layer, AIAA Paper 97-0058 (1997).

[26] Scorer R.S., Davenport L.J., Contrails and aircraft downwash, J. Fluid Mech. 43 (1970) 451–464.

[27] Sipp D., Jacquin L., Cossu C., Self-adaption and viscous selection in concentrated two-dimensional vortex dipoles, Phys. Fluids 12 (2000) 245–248.

[28] Spalart P.R., On the motion of laminar wing wakes in a stratified fluid, J. Fluid Mech. 327 (1996) 139–160.

[29] Spalart P.R., Airplane trailing vortices, Annu. Rev. Fluid Mech. 30 (1998).

[30] Switzer G.F., Proctor F.H., Numerical Study of Wake Vortex Behavior in Turbulent Domains with Ambient Stratification, AIAA Paper 2000-0755 (2000).

[31] Tomassian J.D., The motion of a vortex pair in a stratified medium, Ph.D. Dissertation, Univ. of California, Los Angeles, 1979.

[32] Urbatzka E., Wilken D., Estimating runway capacities of German airports, Transportation Planning and Technology 20 (1997) 103–129.

[33] Widnall S.E., Bliss D.B., Zalay A., Theoretical and experimental study of the instability of a vortex pair, in: Olsen et al. (Eds.), Aircraft Wake Turbulence and its Detection, Plenum Press, 1971, p. 305.